JACC: CLINICAL ELECTROPHYSIOLOGY VOL. 4, NO. 1, 2018

ISSN 2405-500X
http://dx.doi.org/10.1016/j.jacep.2017.08.011

NEW RESEARCH PAPER

Integrated Assessment of Left Ventricular Electrical Activation and Myocardial Strain Mapping in Heart Failure Patients

A Holistic Diagnostic Approach for Endocardial Cardiac Resynchronization Therapy, Ablation of Ventricular Tachycardia, and Biological Therapy

Francesco Maffessanti, PhD,[a] Frits W. Prinzen, PhD,[b] Giulio Conte, MD, PhD,[c] François Regoli, MD, PhD,[c] Maria Luce Caputo, MD,[c] Daniel Suerder, MD,[c] Tiziano Moccetti, MD,[c] Francesco Faletra, MD,[c] Rolf Krause, Dr. rer. nat.,[a] Angelo Auricchio, MD, PhD[a,c]

ABSTRACT

OBJECTIVES This study sought to test the accuracy of strain measurements based on anatomo-electromechanical mapping (AEMM) measurements compared with magnetic resonance imaging (MRI) tagging, to evaluate the diagnostic value of AEMM-based strain measurements in the assessment of myocardial viability, and the additional value of AEMM over peak-to-peak local voltages.

BACKGROUND The in vivo identification of viable tissue, evaluation of mechanical contraction, and simultaneous left ventricular activation is currently achieved using multiple complementary techniques.

METHODS In 33 patients, AEMM maps (NOGA XP, Biologic Delivery Systems, Division of Biosense Webster, a Johnson & Johnson Company, Irwindale, California) and MRI images (Siemens 3T, Siemens Healthcare, Erlangen, Germany) were obtained within 1 month. MRI tagging was used to determine circumferential strain (E_{cc}) and delayed enhancement to obtain local scar extent (%). Custom software was used to measure E_{cc} and local area strain (LAS) from the motion field of the AEMM catheter tip.

RESULTS Intertechnique agreement for E_{cc} was good ($R^2 = 0.80$), with nonsignificant bias (0.01 strain units) and narrow limits of agreement (−0.03 to 0.06). Scar segments showed lower absolute strain amplitudes compared with nonscar segments: E_{cc} (median [first to third quartile]: nonscar −0.10 [−0.15 to −0.06] vs. scar −0.04 [−0.06 to −0.02]) and LAS (−0.20 [−0.27 to −0.14] vs. −0.09 [−0.14 to −0.06]). AEMM strains accurately discriminated between scar and nonscar segments, in particular LAS (area under the curve: 0.84, accuracy = 0.76), which was superior to peak-to-peak voltages (nonscar 9.5 [6.5 to 13.3] mV vs. scar 5.6 [3.4 to 8.3] mV; area under the curve: 0.75). Combination of LAS and peak-to-peak voltages resulted in 86% accuracy.

CONCLUSIONS An integrated AEMM approach can accurately determine local deformation and correlates with the scar extent. This approach has potential immediate application in the diagnosis, delivery of intracardiac therapies, and their intraprocedural evaluation. (J Am Coll Cardiol EP 2018;4:138–46) © 2018 The Authors. Published by Elsevier on behalf of the American College of Cardiology Foundation. This is an open access article under the CC BY-NC-ND license (http://creativecommons.org/licenses/by-nc-nd/4.0/).

From the [a]Center for Computational Medicine in Cardiology, Institute of Computational Science, Università della Svizzera italiana, Lugano, Switzerland; [b]Department of Physiology, Cardiovascular Research Institute Maastricht CARIM, Maastricht University, Maastricht, the Netherlands; and the [c]Division of Cardiology, Fondazione Cardiocentro Ticino, Lugano, Switzerland. The authors

The in vivo recognition of viable tissue, quantification of the scar burden, evaluation of abnormal mechanical contraction, and simultaneous identification of abnormality in left ventricular electrical activation is of paramount importance in several invasive and electrophysiological procedures that may include delivery of biological therapy (1-3), ablation of ventricular tachycardia (4-6), and endocardial cardiac resynchronization therapy (CRT) (7-11). In daily clinical practice, this information is acquired by means of different and complementary cardiac imaging modalities. Among the various cardiovascular imaging modalities, cardiac magnetic resonance (CMR) is the gold standard for both myocardial scar delineation and myocardial strain quantification. Despite technological advancements in the integration of the information retrieved from CMR or 3-dimensional echocardiography to make them available during invasive procedures (i.e., identifying the target for delivery of biological therapy, or the best location of endocardial CRT implantation), these approaches are still error-prone, hampering the spatial accuracy in delivering the therapy. Furthermore, time resolution for strain assessment of CMR is still limited. Finally, a significant number of heart failure patients are excluded from CMR imaging due to nonconditional devices, and the diagnostic accuracy of CMR is jeopardized by device- or lead-related shadowing.

The capability of in vivo objectively quantifying myocardial strain and identifying nonviable myocardium while evaluating electrical activation on a beat-to-beat basis would overcome these limitations. This would constitute a completely novel approach to improve diagnostic capability, possibly delivery of intracardiac therapies, and improve the acute evaluation of the therapy effectiveness. Therefore, the aims of the present study were to: 1) test the accuracy of endocardial strain measurements based on anatomo-electromechanical mapping (AEMM) data compared with CMR; 2) evaluate the diagnostic value of AEMM-based strain measurements in the assessment of myocardial viability; 3) compare the diagnostic value of AEMM-based strain with local unipolar voltages in the delineation of myocardial scar; and 4) to evaluate the accuracy AEMM strain combined with voltages in the identification of myocardial scar.

ABBREVIATIONS AND ACRONYMS

AEMM = anatomo-electromechanical mapping

AUC = area under the curve

CMR = cardiac magnetic resonance

CRT = cardiac resynchronization therapy

E_{cc} = circumferential strain

LAS = local area strain

LGE = late gadolinium enhancement

ROC = receiver-operating characteristic

UEG = peak-to-peak unipolar voltage

ΔUEG = change in peak-to-peak unipolar voltage

METHODS

POPULATION. Thirty-three consecutive patients with moderate-to-severe heart failure referred to the Division of Cardiology, Fondazione Cardiocentro Ticino, Switzerland, for nonpharmacological treatment between 2012 and 2016 were retrospectively included in this study. All patients were on stable drug therapy (>3 months) and underwent standard 12-lead electrocardiography, a clinically indicated CMR study, an electrophysiological study including AEMM of the left ventricle, and coronary angiography. AEMM was performed prior to the implantation of a CRT device in 25 cases or the delivery of biological therapy in 8 cases.

The Institutional Review Board approved the study, and informed consent was obtained before the intervention.

CARDIAC MAGNETIC RESONANCE. CMR was performed using a 3T scanner (MAGNETOM Skyra, Siemens Healthcare, Erlangen, Germany) equipped with a standard torso coil. Steady-state free-precession cine CMR of the left ventricle was acquired in 3 long-axis and in a stack of short-axis slices spanning the left ventricle base to apex (retrospective gating,

gratefully acknowledge financial support by Fondazione Cardiocentro Ticino, the Theo Rossi di Montelera Foundation, the Mantegazza Foundation, and FIDINAM to the Center of Computational Medicine in Cardiology. This work was supported by grants from the Swiss National Science Foundation under project 32003B_165802 and the Swiss Heart Foundation, and by a restricted grant of Biologic Delivery Systems, Division of Biosense Webster, a Johnson & Johnson Company. Patients included were part of the METHOD (Bone Marrow dErived cell Therapy in the stable pHase of chrOnic ischemic heart Disease) clinical trial (NCT01666132). Some of the work presented in the Methods is covered by intellectual property owned by Biosense Webster (U.S. patent "Integrated assessment of electrical activation and myocardial strain," application 15/614,111 filed on June 5, 2017; inventors Angelo Auricchio, Francesco Maffessanti, Frits W. Prinzen, and Hanspeter Fischer). Dr. Prinzen has received research grants from Abbott, Medtronic, St. Jude Medical, Sorin, Merck Sharp & Dohme, Biosense Webster, and Biotronik. Dr. Regoli has received speaker fees from Medtronic, LivaNova, and Boston Scientific; and has served as a consultant for Bayer, Bristol-Myers Squibb/Pfizer, and Daiichi-Sankyo. Dr. Faletra has received speaker fees from Philips Healthcare. Dr. Auricchio has served as a consultant for Medtronic, Boston Scientific, LivaNova, and St. Jude Medical; and has received speaker fees from Medtronic, Boston Scientific, and LivaNova. All other authors have reported that they have no relationships relevant to the contents of this paper to disclose.

All authors attest they are in compliance with human studies committees and animal welfare regulations of the authors' institutions and Food and Drug Administration guidelines, including patient consent where appropriate. For more information, visit the *JACC: Clinical Electrophysiology* author instructions page.

Manuscript received June 5, 2017; revised manuscript received July 25, 2017, accepted August 17, 2017.

temporal resolution 25 to 40 ms, voxel size 1.2 mm × 1.2 mm × 8 mm).

Thereafter, grid-tagged image acquisition was performed using the same slice prescription as for the cine imaging with 6- to 8-mm tag spacing over 25 cardiac phases (temporal resolution 34 to 46 ms).

Finally, short-axis late gadolinium enhancement (LGE) images were obtained 7 to 12 min after the intravenous bolus injection of gadolinium (gadobutrol, 0.2 mmol/kg body weight). Inversion times were adjusted to suppress the signal from the normal myocardium (typical inversion time 200 to 300 ms, voxel size 2 mm × 2 mm × 10 mm). Each short-axis slice was subdivided into 16 angular sectors and was semiautomatically segmented with the full-width half-maximum criterion (12). Local scar extent was defined as the percent of scar in each sector, normalized for the area of the sector.

Circumferential strain (E_{cc}) measurements were obtained from the tagged short-axis CMR images using the SinMod method, with the image in correspondence of the maximum left ventricular volume as temporal reference for strain computation (13).

ELECTROANATOMICAL MAPPING. The electroanatomic mapping system (NOGA XP, Biologic Delivery Systems, Division of Biosense Webster, a Johnson & Johnson Company, Irwindale, California) as well as the navigation and mapping methods have been previously described (14). A set of signal and catheter stability criteria were checked before a measurement point was accepted, following the standardized NOGA XP mapping criteria (15,16).

The phases of the sequentially recorded peak-to-peak unipolar voltage (UEG) and position data were aligned using the simultaneously recorded 12-lead surface electrocardiography.

POST-PROCESSING. Three-dimensional catheter tip displacements were filtered using a moving least square method, as previously described (17), and subsequently expressed as a function of the 3-dimensional DICOM (Digital Imaging and Communications in Medicine) coordinates. Finally, the Lagrangian strain was computed from the displacement field. E_{cc} was obtained as the strain component along the circumferential direction. A simplified measurement of local area strain (LAS), describing the deformation of a small square of tissue, was also computed as the square root of the product between the strain components in the circumferential and longitudinal directions. Finally, both for E_{cc} and LAS, the absolute peak value throughout the systolic phase and end-systolic strain values were considered. The time step corresponding to the largest volume of the surface enclosing all the endocardial points was used as reference for strain computation.

Changes in UEG (ΔUEGs) were measured in a temporal window of 50 ms centered around the local activation time.

REGISTRATION. Endocardial AEMM data were integrated with CMR data offline by a rigid registration algorithm using a 2-step algorithm developed in MATLAB R2014b (MathWorks, Natick, Massachusetts). First, the center of gravity of the points was aligned with the center of gravity of the endocardial cavity segmented from cine CMR end-diastole. Second, an iterative closest-point approach was used to minimize the Euclidean distance between the points and the endocardial contours from CMR.

STATISTICAL ANALYSIS. All data are expressed as mean ± SD or as absolute values and frequency, as appropriate. The relationship between each technique, AEMM- and CMR-derived E_{cc} strain, was evaluated with linear regression analysis and Pearson's correlation coefficient. The agreement between AEMM and CMR reference values was evaluated through the use of Bland-Altman analysis by calculating the bias (mean difference) and the 95% limits of agreement (2 SDs around the mean difference).

The association between scar fraction and peak strain values was measured using linear regression. For each strain variable, the Mann-Whitney *U* test was used to evaluate the significance of the difference between the 2 groups (scar vs. nonscar). Area under the curve (AUC) was determined from receiver-operating characteristic (ROC) curve analysis to determine the ability of AEMM strain measurements to detect the presence of scar (scar fraction >50%) on CMR. The optimal threshold and the corresponding accuracy for each of the considered variables were identified from the ROC curve in correspondence of the point closest to the upper left corner of the ROC plane.

Two-sided p values <0.05 were considered significant.

RESULTS

The clinical characteristics of the patients included in the study are summarized in **Table 1**. None of the patients experienced AEMM-related complications. CMR tagged imaging was not performed in 8 cases due to the clinical condition of the patient at the time of the CMR examination. Patients with and without CMR-tagged imaging were similar (Online Table 1).

VALIDATION OF AEEM-DERIVED STRAIN VERSUS CMR. A total of 25 patients was included for the comparison between AEMM- and CMR-derived

TABLE 1 Patient Characteristics (N = 33)

Age, yrs	69 ± 11
Male	24 (73)
NYHA functional class	
II	16 (48)
III	17 (52)
Etiology	
Ischemic	19 (58)
Idiopathic	14 (33)
QRS duration, ms	153 ± 27
LBBB	21 (64)
Rhythm	
Sinus	30 (91)
Atrial fibrillation	3 (9)
Medications	
ACE inhibitors	30 (91)
Diuretics	26 (79)
Beta-blockers	33 (100)
CMR volumes	
Mass, g	159 ± 38
EDV, ml	270 ± 87
ESV, ml	199 ± 74
EF, %	27 ± 8
LGE CMR scar	
Any scar	22 (67)
Scar extent,	28 ± 17

Values are mean ± SD or n (%).

CMR = cardiac magnetic resonance; EDV = end-diastolic volume; EF = ejection fraction; ESV = end-systolic volume; LBBB = left bundle branch block; LGE = late gadolinium enhancement; NYHA = New York Heart Association.

strains. On average, 194 ± 64 local unique endocardial points were considered and averaged over the standard American Heart Association segments. Acquisition of dense AEMM data covering the whole left ventricular cavity took approximately 40 to 60 min per patient. **Figure 1** depicts a qualitative comparison between AEMM and CMR circumferential strain in a standard mid-left ventricular short-axis plane in a representative patient. Both the AEMM (red) and CMR (blue) curves show a typical pattern of contraction in the circumferential direction, with a systolic downslope (contraction), followed by a diastolic upslope (relaxation). Of note, the peak values between the 2 techniques are very similar, albeit the timing of the peak is not always coincident, and this can be explained by the different temporal resolution between AEMM and CMR. Indeed, the measured deformation refers to a nondeformed configuration, taken in correspondence of the largest left ventricular volume. Although the high temporal resolution for AEMM allowed the accurate identification of the reference configuration in time, the temporal resolution of CMR (25 phases per cardiac cycle) might have resulted in suboptimal identification of the reference for strain computation, introducing a relative delay between the CMR- and AEMM-derived strain curves.

The ripples in the diastolic phase can be explained by fading of the tags on the CMR images that hampers proper tracking. **Figure 2** shows the degree of agreement between AEMM and CMR measurements of E_{cc}, separately for absolute peak (top) and end-systolic values (bottom). AEMM strains were highly correlated to CMR measurements (**Figure 2**, left panels), with Pearson correlation coefficients (R^2) of 0.80 for peak E_{cc} and 0.71 for end-systolic E_{cc}.

The Bland-Altman analysis (**Figure 2**, right panels) shows narrow limits of agreement both for peak and end-systolic values and nonsignificant bias ($p = 1$ both for peak and end-systolic values) compared with the CMR measurements. The slightly larger variation observed for end-systolic E_{cc} can be explained by the different temporal resolution between the 2 techniques, higher for AEMM than CMR, that may preclude the identification of the true end-systolic and end-diastolic time frames, in particular for CMR.

ASSOCIATION BETWEEN SCAR AND STRAIN AMPLITUDE. All the enrolled 33 patients had CMR LGE, and after excluding signals located at the left ventricular base or in the left ventricular outflow tract a total of 4,706 segments (200 ± 56 per patient) were included in the analysis.

The left panels of **Figure 3** depict the relation between the directional strain components and the scar fraction. Despite some intragroup variability, especially in those segments with scar fraction <40%, a significant trend toward reduction in the amplitude of strain was observed. This was evident both for E_{cc} ($r^2 = 0.17$, slope = 0.09, $p < 0.01$ vs. constant model) and LAS ($r^2 = 0.21$, slope = 0.17, $p < 0.01$ vs. constant model).

Using a scar fraction threshold of 50%, 1,457 of the 4,706 segments were classified as scar. Scar segments had significantly lower absolute strain amplitudes compared with nonscar segments in both considered strain variables: E_{cc} (median [first to third quartile], nonscar -0.10 [-0.15 to -0.06] vs. scar -0.04 [-0.06 to -0.02]; $p < 0.01$), and LAS (nonscar -0.20 [-0.27 to -0.14] vs. scar -0.09 [-0.14 to -0.06]; $p < 0.01$). ROC analysis (**Figure 3**, right) showed that AEMM strains accurately discriminated between scar and nonscar segments. LAS was slightly better in identifying significant scar (AUC: 0.84; accuracy = 0.76; for threshold = -0.14) than E_{cc} (AUC: 0.79; accuracy = 73%; for threshold = -0.07).

As expected, ΔUEGs were more significantly reduced in the presence of scar (5.6 [3.4 to 8.6] mV) than in viable myocardium (9.3 [6.4 to 13.0] mV). Nevertheless, the capability of discriminating scar

FIGURE 1 Comparison Between AEMM-Derived and CMR-Derived Circumferential Strain Curves

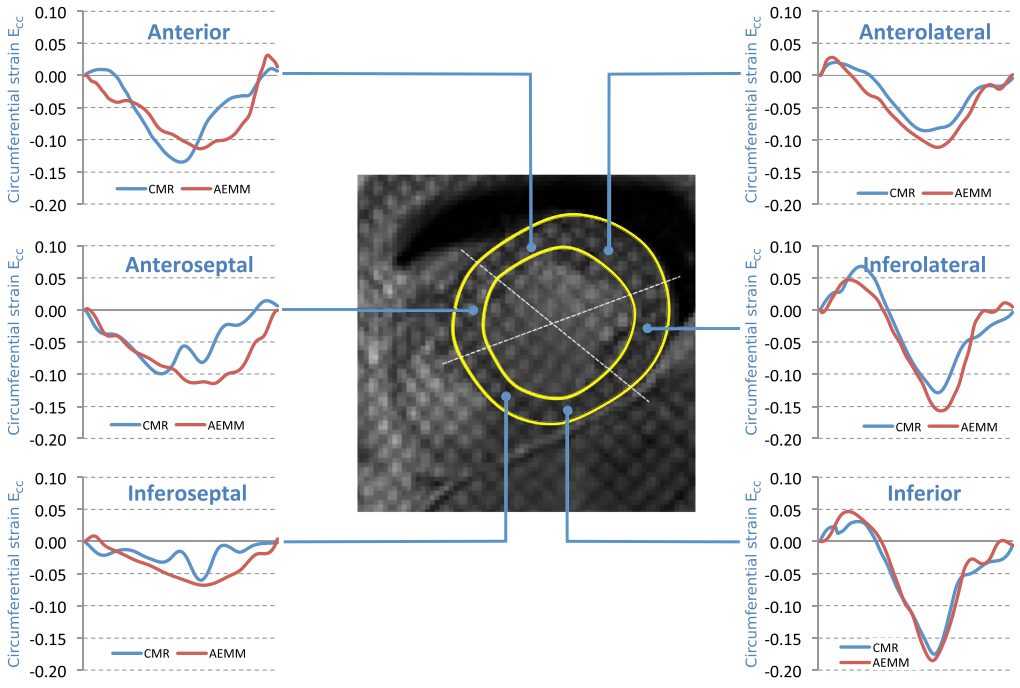

Example of circumferential strain (E_{cc}) curves throughout the cardiac cycle obtained using tagging cardiac magnetic resonance (CMR) **(blue curves)** and anatomo-electromechanical mapping (AEMM) mapping **(red curves)** in a midventricular short-axis slice. Curves are presented for each of the standard American Heart Association sectors.

from nonscar segments (ROC AUC: 0.73) was nonsuperior to any of the considered strain measurements, with an accuracy of 68% using a 7.3-mV threshold.

Using the previously obtained thresholds, the combination of LAS and ΔUEG significantly improved the ability to identify significant scar regions (**Figure 4**), from 68% ΔUEG and 73% using LAS to 83% for the combination of ΔUEG and LAS.

DISCUSSION

The main findings of the study are: 1) the measurement of strains based on AEMM data compared well with strains derived from tagged imaging CMR, the gold standard for clinical myocardial strain assessment; 2) there is a significant, inverse correlation between local peak strain values and scar extent, most evident when considering scar transmurality >50%; 3) LAS and E_{cc} show good diagnostic accuracy in discriminating extensive regional presence of scar (scar extent >50%); and 4) LAS has a significant additional value to clinical used UEGs in the identification of local myocardial scar.

COMPARISON WITH CMR DEFORMATION IMAGING. The good correlation between strain calculated using AEMM and tagged CMR, with no bias and reasonable limits of intertechnique agreement, shows the reliability of the AEMM strain measurements.

Although it is not suitable for diagnostic use given the invasiveness of the mapping, the method we describe in this study has some advantages over CMR. Indeed, in the field of electrophysiology, no intermodality spatial registration or temporal alignment is needed, as the electrical and mechanical signals are acquired at exactly the same time interval in the same spatial location. The temporal resolution for AEMM (100 Hz) is significantly higher than for tagging CMR (usually varying between 20 and 30 images per heartbeat). Furthermore, AEMM can be obtained automatically, without the need for operator-dependent tracing, in quasi-real time, providing the opportunity to evaluate the acute local functional and mechanical response to therapy, for instance, following endocardial CRT or VT ablation. The endocardial strain curves can be easily used to obtain indices of myocardial performance, such as the circumferential

FIGURE 2 **Linear Regression and Bland-Altman Analyses Between AEMM-Derived and CMR-Derived Circumferential Strain**

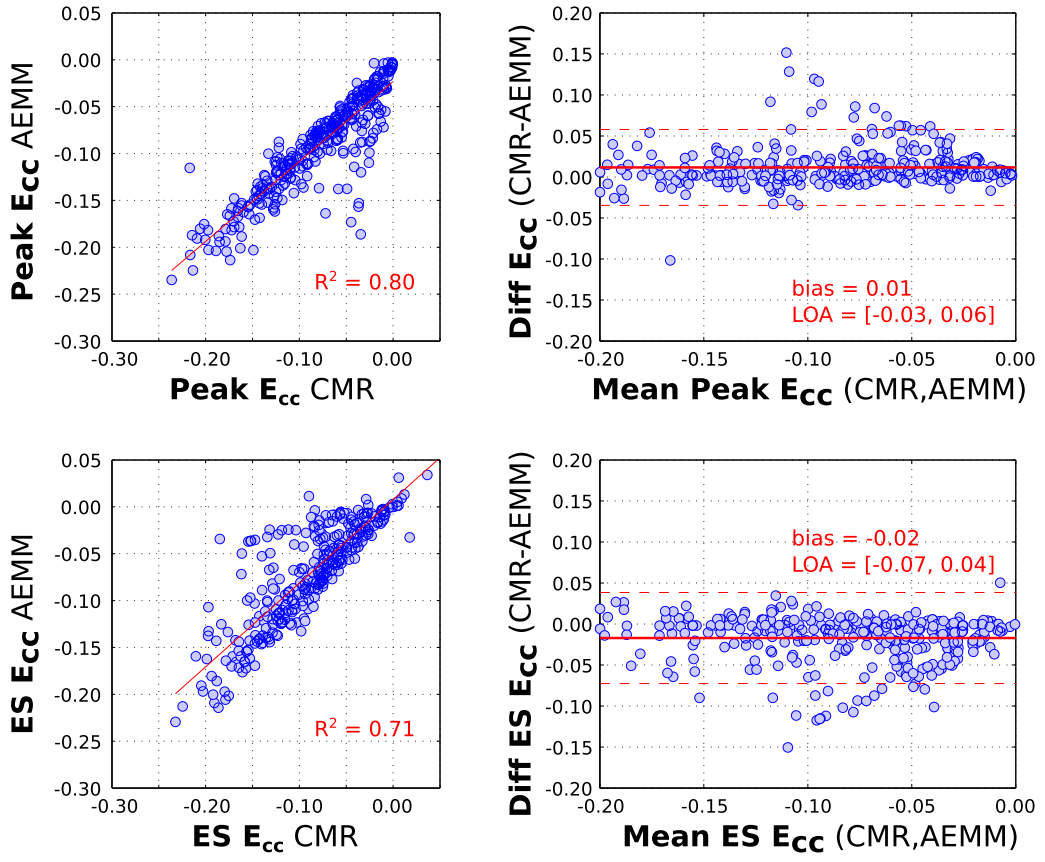

(Left) Results of linear regression analysis (Pearson correlation coefficient R^2) of peak E_{cc} calculated using tagged CMR and AEMM. **(Right)** Results of Bland-Altman analysis of peak E_{cc}. **Thick line** shows the bias, whereas the **thin dashed lines** show the 95% limits of agreement (LOA). Abbreviations as in **Figure 1**.

uniformity ratio (9,18) or the systolic stretch index SSI (19).

Another advantage of AEMM- over CMR-derived strains is that AEMM provides strains over an entire cardiac cycle, whereas taglines fade after approximately half a second, thus making analysis of diastolic strains cumbersome.

Finally, AEMM-derived strain can be obtained in patients not suitable for CMR imaging, whether due to the presence of unconditional devices or the shadowing effects of the already-in-place devices and leads.

Some of the variability between CMR and AEMM strains can be understood from the fact that AEMM strains were computed from the endocardial field of displacement, while tagging used the average mid-myocardial deformation. Moreover, there may be some geometrical uncertainty in matching the CMR with the AEMM data. Radial and longitudinal strain could not be compared between CMR and AEMM, because the endocardial AEMM displacement precluded radial strain calculation by AEMM and because CMR strain calculation from stacks of short-axis images precluded CMR longitudinal measurements. The fact that AEMM- and CMR-determined E_{cc}s matched quite well is important because Helm et al. (20) demonstrated the superiority of circumferential over longitudinal deformation in the quantitative evaluation of the dyssynchronous heart.

SCAR DELINEATION. Deformation abnormalities have been extensively related to ischemia or myocardial scar (21). Therefore, it may come as no surprise that the AEMM-derived strains can recognize scarred regions. The inverse strain-scar relationship was more evident for E_{cc} than for longitudinal strain and was intermediate for LAS. The large spread of strain values observed for moderately scarred segments (<40% scar) might be explained by the variable

FIGURE 3 Association Between Circumferential or Area Strain Values, and Scar Extent

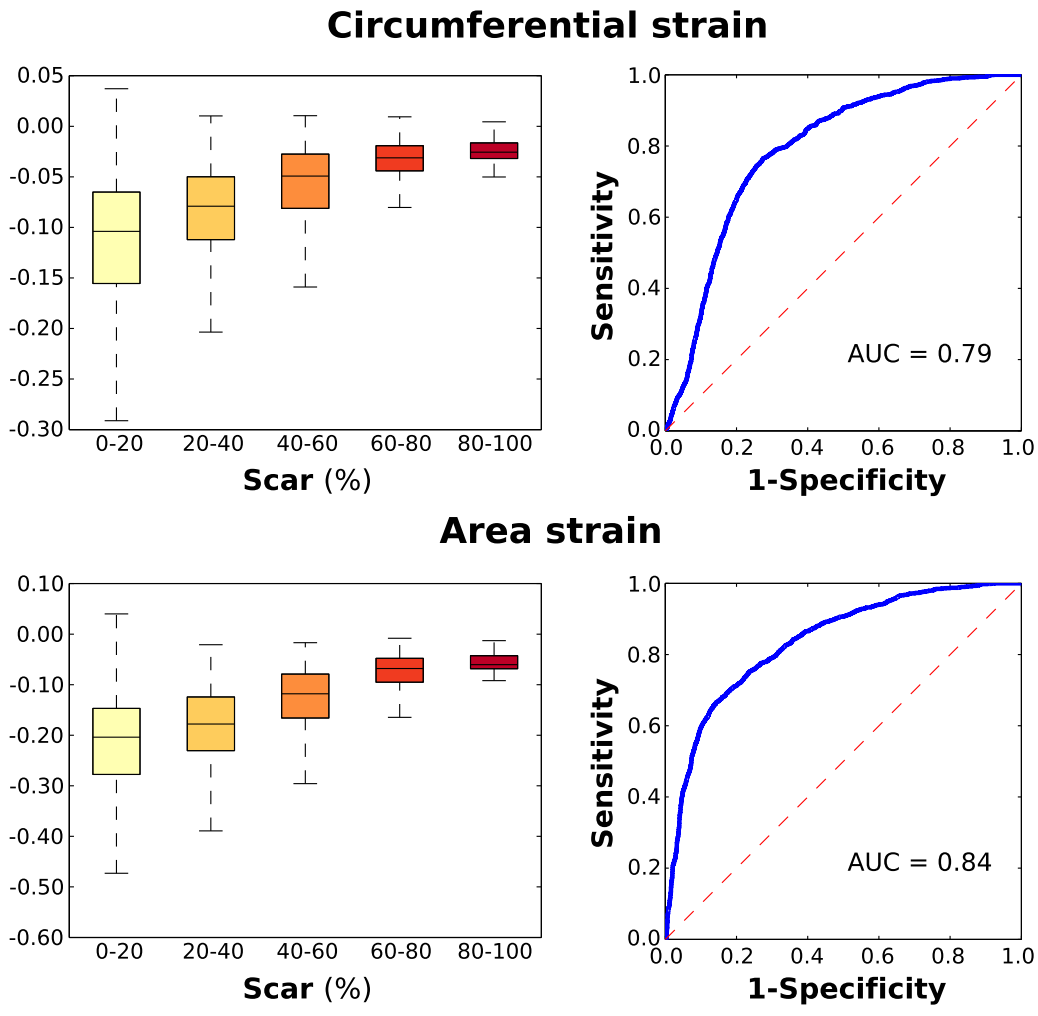

(Left) Distribution of E_{cc} **(top left)** and area strain **(bottom left)** grouped according to scar extent as defined by late gadolinium enhancement CMR. **(Right)** Receiver-operating characteristic curves for strain in the detection of >50% scar extent. AUC = area under the curve; other abbreviations as in Figure 1.

presence of scar or nonscarred tissue surrounding such region, causing variable tethering. The results of our study are consistent with those obtained in a similar study performed by Kihlberg et al. (21), showing a significant correlation between scar extent and strain value, greater for the circumferential than the longitudinal components obtained using DENSE (Displacement Encoding with Stimulated Echoes) CMR sequences. Interestingly, in the same study, the authors proved that in particular circumferential strain is an excellent discriminator between healthy myocardium and scar tissue, when scar is defined as 50% scar in a segment. Also, the diagnostic accuracy reported in the study was very similar among endocardial, transmural, or epicardial strain. These results not only confirm ours, but also support the use of endocardial strain measurements, as achieved from endocardial AEMM mapping.

Interestingly, scar delineation based on strain measurements performed better (LAS AUC: 0.84) than ΔUEGs (AUC = 0.73) in the identification of scar extent >50%. Reduced endocardial voltages are commonly used as surrogate for scar during electrophysiological procedures and for targeting the delivery of biological therapies. Nevertheless, preclinical data focusing on the association between voltage amplitudes showed only moderate correlation between the presence of scar and

FIGURE 4 Distribution of Peak-to-Peak Unipolar Voltages With Respect to Area Strain

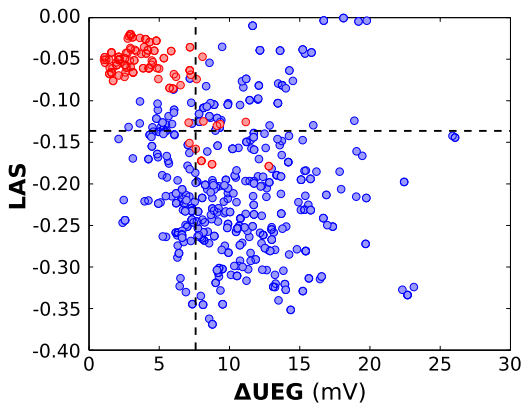

Combined distribution of peak-to-peak local unipolar voltages (ΔUEGs) and local area strain (LAS). Thresholds **(dashed lines)** have been obtained from receiver-operating characteristic curve analysis. See text for details.

reduced peak-to-peak voltages, especially for nontransmural scar, even in well-controlled experimental setups (22).

Although a larger and independent study population is needed to claim the superiority of scar delineation based on mechanical deformation over peak-to-peak voltages, our results suggest how the intraprocedural scar identification could benefit from the combined evaluation of local voltages and strain, presumably in those "gray" areas characterized by nontransmural scar. Indeed, when combining mechanical to peak-to-peak voltages in the detection of scar, using the threshold values independently obtained from the ROC analysis (i.e., defining scar in presence of LAS >-0.14 and ΔUEG <7.3 mV), this resulted in an accuracy equal to 83%, higher than for any variable taken alone.

The possibility to obtain data about electrical, mechanical, and structural (scar) properties of the myocardium will be extremely helpful for developing and improving mathematical models of cardiac function. After all, one of the most challenging tasks in this field is the data-model integration, which in turn strongly relies on the accuracy of multiple-data integration and registration (23).

STUDY LIMITATIONS. The results presented here might have been affected by spatial alignment mismatch, both for the validation against tagged CMR and scar delineation versus LGE imaging, and by temporal misalignment. These methodological limitations are also encountered in clinical routine when merging CMR data with mapping results and could be overcome using the AEMM method proposed here.

Given the retrospective nature of the study and the offline post-processing of the AEMM data, we could not evaluate the feasibility of intraprocedural real-time analysis. However, from a computational perspective the assessment of directional strain takes a few seconds (<3 s) for a complete mapping (approximately 200 points) on a standard laptop.

The low prevalence of isolated epicardial scar not associated with transmural scar (2.4%) in the patient population did not allow evaluation of the accuracy of scar detection separately for the subendocardial, intramural end epicardial layer. Also, dichotomization of myocardial tissue into scar and nonscar prevented investigation of the association between mechanical measurements and gray-zone tissue as from LGE.

Although the method was developed using a NOGA XP mapping system, the same analysis could be performed using other mapping systems based on the same catheter technology, such as the CARTO system (Biosense Webster). Moreover, it may be possible to extract similar strain information using other mapping systems, but this would require further validation. It is important to emphasize that the strain calculation used a novel signal processing approach that spatially filtered the tracing using the moving least squares method to reduce the influence of noise in the strain tracings (17).

CONCLUSIONS

An integrated approach based on AEMM was used to assess, beyond the electrical activation, the local deformation and, indirectly, the scar extent in heart failure patients. The opportunity of objectively quantifying in vivo the mechanical, electrical, and scar properties on a beat-to-beat basis without the need for temporal or spatial intermodality registration constitutes a novel holistic approach with potential immediate application in the diagnosis, delivery of intracardiac therapies, and intraprocedural evaluation of their effectiveness.

ACKNOWLEDGEMENTS The authors sincerely thank Hanspeter Fischer of Biosense Webster for his contribution in data acquisition and for making the data available for offline analysis.

ADDRESS FOR CORRESPONDENCE: Dr. Francesco Maffessanti, Center for Computational Medicine in Cardiology, Università della Svizzera italiana, Via G. Buffi 13, CH-6904 Lugano, Switzerland. E-mail: francesco.maffessanti@usi.ch.

PERSPECTIVES

COMPETENCY IN MEDICAL KNOWLEDGE: The peak-to-peak voltage of the intracardiac electrogram has been usually regarded as a reliable measure of tissue viability and used for the identification of scar. Local myocardial deformation and strain, derived from the motion of the catheter tip, can be accurately measured during electroanatomic mapping. Local strain is a better discriminator between normal and scar regions than is peak-to-peak voltage of intracardiac electrogram.

TRANSLATIONAL OUTLOOK: The proposed AEMM can improve the diagnosis of myocardial scar. Further studies are needed to prove that scar delineation may be further improved by combining the voltage of intracardiac electrogram and ventricular wall deformation, as well as the role of AEMM as guide for the delivery of intracardiac therapies.

REFERENCES

1. van Ramshorst J, Atsma D, Beeres S, et al. Effect of intramyocardial bone marrow cell injection on left ventricular dyssynchrony and global strain. Heart 2009;95:119–24.

2. Pokushalov E, Romanov A, Corbucci G, et al. Cardiac resynchronization therapy and bone marrow cell transplantation in patients with ischemic heart failure and electromechanical dyssynchrony: a randomized pilot study. J Cardiovasc Transl Res 2011;4:767–78.

3. Nelson TJ, Martinez-Fernandez A, Yamada S, Perez-Terzic C, Ikeda Y, Terzic A. Repair of acute myocardial infarction by human stemness factors induced pluripotent stem cells. Circulation 2009;120:408–16.

4. Aliot EM, Stevenson WG, Almendral-Garrote JM, et al. EHRA / HRS Expert Consensus on Catheter Ablation of Ventricular Arrhythmias developed in a partnership with the European Heart Rhythm Association. Europace 2009;11:771–817.

5. Josephson ME, Anter E. Substrate mapping for ventricular tachycardia. J Am Coll Cardiol EP 2015;1:341–52.

6. Ciaccio EJ, Ashikaga H, Kaba RA, et al. Model of reentrant ventricular tachycardia based upon infarct border zone geometry predicts reentrant circuit features as determined by activation mapping. Heart Rhythm 2009;4:1034–45.

7. Leyva F, Foley PWX, Chalil S, et al. Cardiac resynchronization therapy guided by late gadolinium-enhancement cardiovascular magnetic resonance. J Cardiovasc Magn Reson 2011;13:29.

8. Bilchick KC, Kuruvilla S, Hamirani YS, et al. Impact of mechanical activation, scar, and electrical timing on cardiac resynchronization therapy response and clinical outcomes. J Am Coll Cardiol 2014;63:1657–66.

9. Budge LP, Helms A, Salerno M, Kramer CM, Epstein FH, Bilchick KC. Magnetic resonance cine DENSE dyssynchrony parameters for the evaluation of heart failure: comparison to myocardial tissue tagging. J Am Coll Cardiol Img 2012;5:789–97.

10. Ypenburg C, Bommel RJ Van, Delgado V, et al. Optimal left ventricular lead position predicts reverse remodeling and survival after cardiac resynchronization therapy. J Am Coll Cardiol 2008;52:1402–9.

11. Khan FZ, Virdee MS, Palmer CR, et al. Targeted left ventricular lead placement to guide cardiac resynchronization therapy: the TARGET study: a randomized, controlled trial. J Am Coll Cardiol 2012;59:1509–18.

12. Flett AS, Hasleton J, Cook C, et al. Evaluation of techniques for the quantification of myocardial scar of differing etiology using cardiac magnetic resonance. J Am Coll Cardiol Img 2011;4:150–6.

13. Arts T, Prinzen FW, Delhaas T, Milles JR, Rossi AC, Clarysse P. Mapping displacement and deformation of the heart with local sine-wave modeling. IEEE Trans Med Imaging 2010;29:1114–23.

14. Potse M, Krause D, Kroon W, et al. Patient-specific modelling of cardiac electrophysiology in heart-failure patients. Europace 2014;16:iv56–61.

15. Gepstein L, Goldin A, Lessick J, et al. Electromechanical characterization of chronic myocardial infarction in the canine coronary occlusion model. Circulation 1998;98:2055–64.

16. Gyöngyösi M, Dib N. Diagnostic and prognostic value of 3D NOGA mapping in ischemic heart disease. Nat Rev Cardiol 2011;8:393–404.

17. Kroon W, Lumens J, Potse M, et al. In vivo Electromechanical assessment of heart failure patients with prolonged QRS duration. Heart Rhythm 2015;12:1259–67.

18. Bilchick KC, Dimaano V, Wu KC, et al. Cardiac magnetic resonance assessment of dyssynchrony and myocardial scar predicts function class improvement following cardiac resynchronization therapy. J Am Coll Cardiol 2008;1:561–8.

19. Lumens J, Bhupendar T, Walmsley J, et al. Differentiating electromechanical from non-electrical substrates of mechanical discoordination to identify responders to cardiac resynchronization therapy. Circ Cardiovasc Imaging 2015;8:e003744.

20. Helm RH, Leclercq C, Paris OP, et al. Cardiac dyssynchrony analysis using circumferential versus longitudinal strain: Implications for assessing cardiac resynchronization. Circulation 2005;111:2760–7.

21. Kihlberg J, Haraldsson H, Sigfridsson A, Ebbers T, Engvall JE. Clinical experience of strain imaging using DENSE for detecting infarcted cardiac segments. J Cardiovasc Magn Reson 2015;17:50.

22. Pavo N, Jakab A, Emmert MY, et al. Comparison of NOGA endocardial mapping and cardiac magnetic resonance imaging for determining infarct size and infarct transmurality for intramyocardial injection therapy using experimental data. PLoS One 2014;9:e113245.

23. Chabiniok R, Wang VY, Hadjicharalambous M, et al. Multiphysics and multiscale modelling, data-model fusion and integration of organ physiology in the clinic: ventricular cardiac mechanics. Interface Focus 2016;6:20150083.

KEY WORDS cardiac magnetic resonance, electromechanical mapping, endocardial mapping, heart failure, scar tissue, strain imaging

APPENDIX For a supplemental table, please see the online version of this paper.